Journal Pre-proof

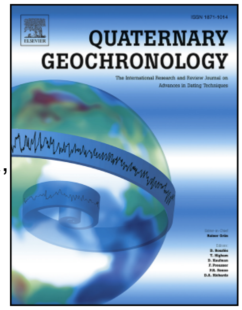

Constraining the age of the Pleistocene sedimentary infill of Cueva Mayor (Atapuerca, N Spain) through a multi-technique dating approach.

V. Martínez-Pillado, M. Demuro, J.E. Ortiz, Q. Shao, L.J. Arnold, M. Duval, H. Cheng, T. Torres, E. Santos, C. Falguères, O. Tombret, N. García, A. Aranburu, A. Gómez-Olivencia, J.L. Arsuaga

PII: S1871-1014(24)00080-3

DOI: https://doi.org/10.1016/j.quageo.2024.101576

Reference: QUAGEO 101576

To appear in: *Quaternary Geochronology*

Received Date: 15 November 2023

Revised Date: 14 June 2024

Accepted Date: 23 June 2024

Please cite this article as: Martínez-Pillado, V., Demuro, M., Ortiz, J.E., Shao, Q., Arnold, L.J., Duval, M., Cheng, H., Torres, T., Santos, E., Falguères, C., Tombret, O., García, N., Aranburu, A., Gómez-Olivencia, A., Arsuaga, J.L., Constraining the age of the Pleistocene sedimentary infill of Cueva Mayor (Atapuerca, N Spain) through a multi-technique dating approach., *Quaternary Geochronology*, https://doi.org/10.1016/j.quageo.2024.101576.

Constraining the age of the Pleistocene sedimentary infill of Cueva Mayor (Atapuerca, N Spain) through a multi-technique dating approach.

V. Martínez-Pillado[1,2]*, M. Demuro[3], J.E. Ortiz[4], Q. Shao[5], L.J. Arnold[3], M. Duval[2,6,7], H. Cheng[8], T. Torres[4], E. Santos[1], C. Falguères[9], O. Tombret[9], N. García[10], A. Aranburu[11], A. Gómez-Olivencia[1,11,12], J.L. Arsuaga[1,9]

[1]Centro Mixtro UCM-ISCIII sobre Evolución y Comportamiento Humanos. Madrid, Spain.
[2] Centro Nacional de Investigación sobre la Evolución Humana (CENIEH). Burgos, Spain.
[3] School of Physics, Chemistry and Earth Sciences, Institute for Photonics and Advanced Sensing (IPAS), Environment Institute, University of Adelaide, Australia.
[4]Departamento Ingeniería Geológica y Minera. E.T.S. de Ingenieros de Minas y Energía. Madrid, Spain.
[5]College of Geographical Science, Nanjing Normal University, 210023, Nanjing, China
[6] Australian Research Centre for Human Evolution (ARCHE), Griffith University, Brisbane, Australia.
[7]Palaeoscience Labs, Dept. Archaeology and History, La Trobe University, Melbourne Campus, Bundoora, 3086, Victoria, Australia.
[8] Institute of Global Environmental Change, Xi'an JiaotongUniversity, Xi'an, China
[9]UMR 7194 HNHP Histoire Naturelle de L'Homme Préhistorique, MNHN-CNRS-UPVD, Paris, France
[10]Departamento de Geodinámica, Estratigrafía y Paleontología, Universidad Complutense de Madrid, Spain.
[11]Departamento de Geología, Facultad de Ciencia y Tecnología, Universidad del País Vasco-Euskal Herriko Unibertsitatea (UPV/EHU). Leioa, Spain
[12]Sociedad de Ciencias Aranzadi. Donostia, Spain.
*Corresponding author: vmpillado@gmail.com

Abstract

Establishing chronologies of archaeological sites by using a single dating method may not always reliably constrain the age of a deposit or a fossil, as potential biases may naturally arise, particularly in complex sedimentary settings such as caves. In this study, we performed a multi-technique dating approach that targets different materials in two caves from the Cueva Mayor-Cueva del Silo karst system, Sierra de Atapuerca, Spain. Two new fossil teeth from lithostratigraphic unit LU4 (GE-I pit) at Galería de las Estatuas have been dated by combined U-series/ESR and Amino Acid Racemisation (AAR) methods. The former provides ages of 87 ± 9 and 117 ± 13 ka that agree with previous dating studies of this Neandertal site, confirming the assignment of level LU4 to Marine Isotope Stage (MIS) 5. In contrast, AAR analyses produce very scattered ages, pointing to significant post-burial chemical modifications in dentine. A first set of ages is presented for the Cata Litario pit at Sala de los Cíclopes, a palaeontological site formed exclusively of cave bear fossils belonging to the Middle Pleistocene species *Ursus deningeri*. We provide U-series/ESR and AAR ages for two bear teeth from lithostratigraphic unit LU5, and extended-range luminescence ages for the sediment deposits that host, and immediately underlie and overlie, the bear accumulation. Depositional ages of the sediment were obtained using single-grain thermally-transferred optically stimulated luminescence (TT-OSL) dating of individual quartz grains and post-infrared-infrared stimulated luminescence (pIR-IR) dating of K-feldspars. Several speleothems, both *in situ* and reworked fragments embedded in the different lithostratigraphic units, have additionally been dated by U-series to constrain the timing of the sequence formation. The results indicate that the sediment originally entered the cave between MIS-12 and MIS-10 (444 ± 28 ka to 367 ± 32 ka). Nevertheless, the AAR and U-series/ESR fossil ages, as well as some of the speleothem fragment ages from LUs 5 and 6 are significantly younger. Leaving aside methodologically questionable results for one of the bear tooth samples, the most reliable AAR and U-Series/ESR ages range from 256 ± 24 to 287 ± 23 ka, while the speleothem fragments indicate several formation episodes between 444 ± 19 and 284 ± 8 ka. The apparent difference between the U-Series/ESR ages on the fossils and the luminescence ages on the host sediment are not likely to be wholly explained by uncertainties on uranium uptake modelling or gamma dose rate evaluation, and thus is most likely related to taphonomic processes or a complex site formation history.

The presence of fossils and eroded speleothem clasts of younger age within these levels is consistent with either an event of prior erosion, transport and resedimentation of LUs 4, 5 and 6, and/or a complex post-depositional mixing history for the stratigraphic sequence at Cata Litario. This study highlights the importance of using different dating methods to reconstruct reliable chronological frameworks, and to understand the geological factors that can affect the dated materials. This includes the accumulation and taphonomic histories of fossils, post-depositional mixing or reworking processes affecting sediments during the residence time within the karst system.

Keywords: Electron Spin Resonance, Aspartic Acid Racemization, Luminescence, U-series, Atapuerca, Pleistocene.

1. Introduction

The Sierra de Atapuerca (Burgos, N Spain) hosts a unique archaeo-paleontological record that spans the last 1.2 Ma (e.g., Arnold et al., 2014, 2015; Arnold and Demuro, 2015; Arsuaga et al., 2014; Carbonell et al., 1995, 2008, 2014; Demuro et al., 2014, 2022; Rodríguez et al., 2011), offering an unprecedented opportunity for the study and understanding of human evolution in western Europe during the Pleistocene. Besides the world-famous paleoanthropological sites of Sima del Elefante, Gran Dolina and Sima de los Huesos, which have been extensively studied over the last 40 years, the Atapuerca karstic complex also documents a number of sites that have received comparatively less attention, such as Galería de las Estatuas and Sala de los Cíclopes, located within the Cueva Mayor-Cueva del Silo cave complex. This is the largest cave complex in the Atapuerca karst system and contains important sites such as Sima de los Huesos (Arsuaga et al., 2014, 2015) and Portalón (Carretero et al., 2008), among others. These two key sites, located around half a kilometre apart in the extremities of the cave complex, document the largest human fossil assemblage from the Middle Pleistocene and intensive human occupations during the Holocene, respectively. However, the archaeo-palaeontological record within internal sectors of Cueva Mayor-Cueva del Silo (i.e., those far from the current entrances) is scarce, although silos dating to the Holocene have been found in most of these galleries. As such, the timing of human occupations within the cave complex during the Pleistocene and their synchronicity with the presence of other cave-dwelling large mammals, such as bears, remains to be fully understood. While several recent studies have provided some much-needed numerical ages in this regard (Arnold et al., 2014; Demuro et al., 2019a, 2019b; Moreno et al., 2022), the present work contributes with new chronological information for two sites within Cueva Mayor: Galería de las Estatuas and Sala de los Cíclopes. Dating results were obtained through a multi-technique approach including combined Uranium-Series/Electron Spin Resonance (ESR), Amino Acid Racemisation (AAR), Luminescence and U-series dating applied directly to fossils, host sediment and associated carbonate formations. In particular, direct dating of fossil remains using two different methods can provide crucial insights into post-depositional uptake histories and diagenetic complications experienced by dental tissues.

2. Study context

The Sierra de Atapuerca is located 15 km to the east of the city of Burgos, in the Corredor de la Bureba, a natural pass between the basins of the Duero and Ebro rivers, (Fig. 1A). This low-altitude ridge (1078 m) in the Arlanzón River Valley contains a large number of karstic cavities formed within the Upper Cretaceous limestones and dolostones (Fig. 1B), and which have been filled by various sediment types. The largest known cave complex in the Atapuerca karst system is Cueva Mayor-Cueva del Silo, which extends for 4 km and contains three karstic levels that formed during different time periods (Ortega Martínez, 2009) (Fig. 1C). Cueva Mayor hosts many archaeo-palaeontological sites within its galleries, including Galería de las Estatuas, Sala de los Cíclopes, and Sima de los Huesos, the world's largest Middle Pleistocene human fossil accumulation dated between 430 and 300 ka (Arnold et al., 2014; Arsuaga et al., 2014; 2024; Demuro et al., 2019b).

2.1. Galería de las Estatuas

The Galería de las Estatuas site is located in the upper level of the Cueva Mayor-Cueva del Silo karst system (Fig. 1C, D) and is currently isolated from the exterior by detrital sediments and speleothems clogging the nearby entrance. The sedimentary sequence is composed of a combination of chemical carbonate precipitates (speleothems) and >2 m-thick detrital sediments (Aranburu et al., 2012; Arsuaga et al., 2017). Two test pits (GE-I and GE-II) have been excavated since 2008 and have yielded a large amount of faunal remains and Middle Palaeolithic stone tools (Arsuaga et al., 2017), one Neandertal skeletal remain (a distal foot phalanx; Pablos et al., 2019), and sedimentary mitochondrial and nuclear DNA indicating the presence of different Neandertal populations over time (Vernot et al., 2021).

Five lithostratigraphic units (LUs) have been described in the GE-I section, which is delimited both at the base and top by a speleothem deposit (Aranburu et al., 2012; Arsuaga et al., 2017; see Supplementary Information for LUs description). This 2-m thick sedimentary assemblage has been dated by a combination of single-grain quartz optically stimulated luminescence (OSL), single-grain quartz thermally transferred OSL (TT-OSL) (Demuro et al., 2019a) and combined U-series/ESR (Moreno et al., 2022) to 112-80 ka, correlated to marine isotope stage (MIS) 5 (Lisiecki and Raymo, 2005). The underlying speleothem is an ancient flowstone formed towards the east wall of the cave (Aranburu et al., 2012) and seems to correlate to the Matuyama Chron (>0.774 Ma; Parés et al., 2016). In contrast, the most recent phase of chemical precipitation, which includes significant development of stalagmites that seals the sedimentary infill sequence, has been dated by U-series to ~14 ka in GE-I (Martínez-Pillado et al., 2014) and ~54 ka at its base in GE-II (Vernot et al., 2021).

2.2. Sala de los Cíclopes

The Sala de los Cíclopes is located in the intermediate level of the Cueva Mayor-Cueva del Silo system (Fig. 1C, D). This chamber is situated below the margin of the Cretaceous limestones of the Sierra de Atapuerca, right in the contact zone with the overlying Miocene marls (Fig. 2A) (Ortega Martínez, 2009; Ortega et al., 2014). The Sala de los

Cíclopes has an elongated morphology with a marked NNE-SSW direction and is almost 40 m in length, 10 m wide, and its maximum height surpasses 13 m. Gravimetric and magnetometric studies on sediment above the cave suggest an ancient entrance at the bottom of the southern wall of Sala de los Cíclopes, a short passage called Sala de las Oseras (the "bear-bed chamber"), which was subsequently obstructed by cave breakdown (Bergamín et al., 1994). Sediment remnants, mostly fluvial sands and silts, and colluvial red-matrix breccia, are observable as patches on the walls and ceiling of the chamber, as well as on the floor. These remnants evidence a previous infill of the entire cavity that started during the palaeomagnetic Matuyama Chron (>0.774 Ma; Parés et al., 2010), and subsequent emptying, likely due to inflow of water that eroded and transported these materials (Arsuaga et al., 1997; Aranburu et al., 2007; Ortega Martínez, 2009; Ortega et al., 2005; 2014). A 2 m^2 test pit excavated in the central sector of the cavity, called Cata Litario (CL), uncovered a 2-m thick sediment sequence composed of six clayey lithostratigraphic units (LU3 to LU7, from top to bottom) resting on a basal level of white marls (LU8; Fig. 2B). The stratigraphic sequence is covered by a speleothem in the eastern profile that evolves into purple silty-clay facies to the west (LU2), and a layer of guano that covers the entire floor of the room, belonging to the uppermost LU1 (Aranburu et al., 2007; see Supplementary Information for further description of each LU). Lithostratigraphic unit 5 (LU5) contains an important palaeontological assemblage formed exclusively of cave-bears belonging to the Middle Pleistocene species *Ursus deningeri* (García et al., 1997). No other macrofossils or stone tools have been found in Cata Litario or elsewhere in Sala de los Cíclopes. Since fossils of the Late Pleistocene descendant species *Ursus spelaeus* are lacking, it seems likely that this part of the cave ceased to be accessible before the end of the Middle Pleistocene (Arsuaga et al., 1997; García et al., 1997). It is hypothesised that both the humans of the Sima de los Huesos and the bears gained access to the interior of the karst system through an entrance, now sealed off, to the Sala de los Cíclopes, which has not yet been found. Another possibility is that these Middle Pleistocene bear populations entered the cave through the Sima del Elefante entrance and along the Galería Baja, which connects to the Sala de los Cíclopes and is located <500 m away (Fig. 1D). This interpretation is supported by the preservation of bear beds along the Galería Baja. If the Cata Litario sedimentary sequence is interpreted as predating the closing of the Sima del Elefante/Galería Baja palaeoentrance, which is currently completely filled by sediment, its age could be inferred to be older than

200 ka (Demuro et al., 2022). However, there is no chronological data directly available for the sequence to assess this hypothesis.

>Figure 1<

3. Material and methods

3.1 Samples

Four fossil teeth were selected in this study for direct dating using combined U-series/ESR and Amino Acid Racemisation (AAR) methods: two from LU4 of GE-I pit at Galería de las Estatuas (#738 and #739) and another two from LU5 of Cata Litario at Sala de los Cíclopes (#737 and #852) (Figs. S1, S2A,B, Table S1). Two *in situ* gamma spectrometry measurements were made in Cata Litario (Fig. S2B) for sample #737 and four additional sediment samples were collected for laboratory dosimetry evaluation of samples #737 and #852 (see Supplementary Information for further information). In contrast, no *in situ* gamma dose rate measurements were performed at Galería de las Estatuas, since the previous evaluation made for level LU4 (OSL sample GE16-5) by Demuro et al. (2019a) can be directly used for teeth #738 and #739.
In total, four luminescence dating samples were also collected from various units in Cata Litario, namely LU6 (CL16-4), LU5 (CL16-1 and CL16-3) and LU4 (CL16-2) (Fig. S2C,D, Table S1). Samples were collected by hammering PVC tubes into the section, and additional bulk sediment (200 g) was collected from material directly surrounding each sample for the purpose of dosimetry and moisture content evaluations.

Five speleothems (Fig. S2C,D, Table S1) were also sampled from Cata Litario for U-series dating purposes. However, only one of these speleothem samples has been found in an *in situ* position: SCI18-A extracted mechanically from the flowstone forming LU2 and sealing the detritic sequence. In contrast, the other four samples are from two flowstones (SCI18-B and SCI23-B) and two stalagmite fragments (SCI23-A and SCI23-C) collected during the paleontological excavation. SCI18-B and SCI23-A were found in LU6 while SCI23-B and SCI23-C were found inside LU5. These fragments, eroded and embedded in the sediments, are potentially reworked from another part of the cave or have been displaced vertically in the vicinity of Cata Litario. Two subsamples (base and top) were dated for the larger stalagmite (SCI23-C) to chronologically constrain its development.

>Figure 2<

3.2 Combined U-series/ESR dating of fossil teeth

Fossil teeth were dated through a combination of uranium-series and ESR (see Duval, 2015 for further details about the method). Samples were prepared following standard ESR dating procedures for enamel powder (e.g., Duval et al., 2019). ESR analyses of the enamel samples were carried out at CENIEH, Spain, using the multiple aliquot additive dose (MAAD) method, after splitting each enamel sample into 10 to 12 aliquots (Table S2). Solution U-series analyses of dental tissues were performed with a Neptune MC-ICPMS at Nanjing University, with chemical and measurement procedures as in Douville et al. (2010) and Shao et al. (2019), respectively. The environmental dose rate from the sedimentary surroundings was evaluated through a combination of *in situ* and laboratory measurements. Combined U-series/ESR age calculations were performed with DATA (Grün, 2009), a DOS-based program using the US and CSUS models defined by Grün et al. (1988) and Grün (2000), while the USESR program (Shao et al., 2014) was also used for the US and AU model calculations (Shao et al., 2012) (Table S3). Full details of the analytical procedure are given in the Supplementary Information.

3.3 AAR dating of fossil teeth

The same four fossil teeth (#737, #738, #739 and #852) were also independently dated by AAR. This technique calculates the age of an animal's death by assessing the extent of post-mortem conversion of typical biological chiral forms of amino acids (laevorotatory: L-enantiomers) to their dextral counterparts (D-enantiomers) (Bada and Protsch, 1973).

After preparation of the teeth and separation of the dental tissues for U-series and ESR analyses, a portion of the powdered dentine was selected to carry out AAR analyses. Two subsamples of each tooth (Table S5) were subjected to dialysis following Marzin (1990). Dating analyses were carried out at the Laboratory of Biomolecular Stratigraphy (LEB) of the Universidad Politécnica de Madrid, Spain. The amino acid concentrations and ratios were measured using a high-performance liquid chromatograph (HPLC) Agilent-

1100, following the protocol described by Torres et al. (2014). The age of the sample was established by inserting the aspartic acid D/L values into the age calculation algorithm available for dentine collagen samples from the Iberian Peninsula (Torres et al., 2014). A mean AAR age and associated one standard deviation uncertainty was calculated for teeth that returned consistent ages from the two subsamples. Full details of the dating procedure can be found in the Supplementary Information.

3.4 Luminescence dating

The luminescence samples from Cata Litario have been dated using both potassium feldspar pIR-IRSL and quartz TT-OSL signals. Detailed descriptions of the luminescence dating procedures and instrumentation employed are provided in the Supplementary Information. The 90-125 µm fractions of potassium feldspar and quartz grains were extracted, and HF etched, using standard preparation procedures (Aitken, 1998), with the exception of sample CL16-4, for which the 63-90 µm fractions was used. Multi-grain pIR-IRSL$_{225}$ and single-grain TT-OSL measurements were made using the single-aliquot regenerative-dose (SAR) protocol (Murray and Wintle, 2000) detailed in Arnold et al. (2014, 2019) and Demuro et al. (2015, 2022), and shown in Table S6a-b. The pIR-IRSL procedure makes use of raised temperature stimulation at 225ºC after a preheat of 250ºC for 60 s and is herein denoted pIR-IRSL$_{225}$. Dose recovery tests were undertaken on the feldspar pIR-IRSL$_{225}$ and the quartz TT-OSL signals of sample CL16-4 to confirm the suitability of these SAR procedures for D_e determination. The dose recovery test procedures are outlined in the Supplementary Information and the results are shown in Table S7 and Table S8. Final D_e estimation and age calculation was determined using grains or aliquots that passed the SAR quality assurance criteria described in the Supplementary Information. Representative burial dose estimates have been calculated using the central age model (CAM), and the 3-parameter and 4-parameter minimum age models (MAM-3 and MAM-4) of Galbraith et al. (1999). The choice of model to use for the final age calculations has been made on statistical grounds using the overdispersion parameter (calculated using the CAM) and the maximum log likelihood, L_{max}, criterion of Arnold et al. (2009) (to ascertain the statistical appropriateness of the MAM-3 versus MAM-4), and by taking into consideration the depositional context of these samples within a cave setting (e.g., Arnold et al., 2019, 2022), as well as the different bleaching characteristics of the various luminescence signals under consideration (e.g., Arnold et al., 2013; Demuro et al., 2015; Duval et al., 2017).

Environmental doses were determined via a combination of *in situ* field gamma-ray spectrometry and low-level beta counting (Table S9). The field gamma spectra were analysed using the 'energy windows' method described in Arnold et al. (2012a) and Duval and Arnold (2013) to determine radionuclide concentrations of K, U and Th of surrounding sediment. Gamma dose rates have been calculated using the conversion factors of Guérin et al. (2011). Beta dose rates have been derived from laboratory measurements of homogenised sediment sub-samples using a Risø GM-25-5 beta counter. Contributions from cosmic rays have been calculated using the approach described in Prescott and Hutton (1994). High-resolution gamma spectrometry measurements have additionally been made to assess the state of secular equilibrium in the ^{238}U and ^{232}Th decay series for all samples (Table S10).

3.5 U-series dating

Except for sample SCI23-C, one powder subsample of each speleothem was extracted at the University of the Basque Country facilities using a microdrill and tracing the lamination of the speleothem growth. SCI23-C is a fragmented and eroded but well-developed stalagmite of about 25 cm in height (Fig. S2), and two subsamples were taken, one from the base (SCI23-C1) and one from the top (SCI23-C2). Solution U-series dating of the powdered samples was performed at the Isotope Laboratory, Xi'an Jiaotong University using a Multi-Collector Inductively Coupled Plasma Mass Spectrometer (MC-ICP-MS) (Thermo-Finnigan Neptune-plus). Standard chemistry procedures were used to separate U and Th for dating (Edwards et al., 1987). The isotopic measurements were carried out following the methodology of Cheng et al. (2013). Further details about the analytical procedure may be found in the Supplementary Information.

4. Results

4.1 Combined U-series/ESR dating of fossil teeth

4.1.1. General observations on the ESR and U-series data

ESR dose response curves are displayed in Fig. 3A. Overall, the ESR measurements show mean ESR intensities with a variability of 0.8 to 1.8 %, resulting in a D_E precision of 0.5 to 7.2 % (Table S2). The various fitting sensitivity tests performed on the ESR dataset return very close dose estimates, within ± 5% for all but one case (Table S2). Consequently, the robustness of the D_E estimates is supported by the high repeatability of the ESR measurements and the limited influence of D_{max} adjustment, baseline correction, noise intensity correction and data weighting option (Table S2). Final dose evaluation using noise-subtracted and baseline-corrected ESR intensities return D_E estimates of ~47 Gy for #738 and #739, ~239 Gy for #737, and ~314 Gy for #852.

Apparent U-series ages obtained for both enamel and dentine of the two teeth from Galería Estatuas range between ~18 and ~45 ka. However, the cement from #738 yields a much older age of ~96 ka (see Table S3), possibly resulting from a more recent uranium leaching overprint. A similar observation can be made for the dentine of #737, while the other samples from Cata Litario return closer apparent U-series ages of 120 to 140 ka.

4.1.2. Galería de las Estatuas (Pit I)

A combined U-series/ESR age of 90 ± 9 ka can be calculated using the US model of the DATA program for #739, while the USESR program returns a US-ESR estimate of 87 ± 9 ka (Table 1), demonstrating that both softwares return very close ages when using the same data inputs. In contrast, no finite U-series/ESR age can be obtained for #738 with DATA, whereas the use of the USESR (which may offer a slightly higher computational tolerance limits compared to DATA; Shao et al., 2014) yields a US-ESR age of 117 ± 13 ka for this tooth. The use of other uranium uptake models, such as AU or CSUS, results in very minor variation (< 2 ka) in the calculated age for #738 (Table 1), showing the limited impact of uranium uptake modelling for this sample. To sum up, the various combined U-series ages obtained for the two teeth from LU4 range from 87 ± 9 ka to 117 ± 13 ka and agree with each other at the 2σ confidence level (Table 1).

4.1.3. Cata Litario (Sala de los Cíclopes)

It is not possible to calculate a combined U-series/ESR age for tooth sample #737 from the LU5 of Cata Litario with the original U-series data because the dentine is in secular equilibrium (Table S3) and lies beyond the limits of both the DATA and USESR programs when combining the ESR and U-series data, even when using the AU model for the (significantly) older apparent U-series age most likely results from a more recent leaching overprint in that tissue. However, by fixing the uptake parameter $p_{dentine}$ = -1 (i.e., considering a closed system in the dentine), an age of 217 ± 22 ka may be tentatively obtained with DATA. Our age sensitivity tests using different combinations of uranium uptake models (AU and US) with USESR return very close age estimates (217 ± 21 ka and 227 ± 20 ka), indicating that the existing uncertainty on the uranium uptake modelling has a minor impact on the calculated U-series/ESR ages (Table 1). A maximum age of 245 ± 31 ka may be obtained with the CSUS model. Additionally, following the previous work by Arsuaga et al. (2014) on another Middle Pleistocene bear tooth from the Sima de los Huesos, the adjacent cavity to Sala de los Cíclopes, we ran additional age calculations by considering a similar post-Rn disequilibrium in the U-238 decay chain of the dental tissues (^{222}Rn/^{230}Th = 0.30 ± 0.03 in enamel; ^{222}Rn/^{230}Th = 0.20 ± 0.02 in dentine): the resulting ages become 50-60 ka older, between 273 ± 28 and 304 ± 33 ka (Table 1). To sum up, our best estimate for the age of #737 fossil from LU5 of Sala de los Cíclopes lies somewhere between 217 ± 22 ka and 304 ± 33 ka, though a more complex U-series uptake history, such as a succession of repeated uptake-leaching events caused by periodic ponding events in caves, cannot be excluded for this sample. Further investigation would be required in order to properly evaluate how this potential complication would specifically impact the dose rate modelled for the dental tissues.

In contrast, no uranium leaching is observed in the dental tissues of tooth #852 from the same LU5, whose apparent U-series ages range between ~124 and ~134 ka (Table S3). A finite US-ESR age of 258 ± 21 ka can be calculated using the US model of the DATA program (256 ± 24 ka with USESR), while the use of the CSUS model returns a maximum age constraint of 273 ± 21 ka (Table 1). Considering post-Rn disequilibrium in dental tissues following Arsuaga et al. (2014), very close US-ESR and CSUS ages of 280 ± 23 and 287 ± 23 ka respectively (Table 1) are obtained. We can therefore confidently conclude that the true age for tooth #852 lies between 256 ± 24 and 287 ± 23 ka, which is consistent with the range proposed earlier for #737.

>Table 1<

4.2 AAR dating of fossil teeth

Analytical results are summarised in Table S5, which includes the D/L ratios of the relevant amino acids and the total content of each enantiomer, while age results are given in Table 1.

<u>4.2.1. Galería de las Estatuas (Pit I)</u>

The two teeth from Galería de las Estatuas (#738 and #739) yield ages ranging from 56 to 175 ka. In particular, the two subsamples of #738 produce very scattered ages differing by ~100 ka (76 and 175 ka; Table 1), whereas the replicate ages of #739 are much less scattered (differing by 11 ka) and cluster around 60 ka. Taken individually, these results differ significantly from the U-series/ESR ages obtained from the same teeth, as well as from the previous dating results on unit LU4 (Demuro et al., 2019a; Moreno et al., 2022). Such discrepancy most likely results from the high concentration of some amino acids, such as Alanine (in red in Table S5), which indicates a post-burial chemical (i.e., diagenetic) modification of the tissues (e.g., Laabs and Kaufman, 2003; Kosnik and Kaufman, 2008). Consequently, the reliability of the AAR results obtained from samples #738 and #739 may be reasonably questioned from a methodological perspective. These age estimates are therefore not considered further in the discussion around the chronology of the sedimentary infill of Galería de las Estatuas. A more detailed study of the amino acid ratios for these two samples is needed to determine the taphonomic processes that caused the AAR inaccuracy.

4.2.2. Cata Litario (Sala de los Cíclopes)

The aspartic acid concentrations and Asp D/L values give an average age of 378 ± 14 ka for #737 from Cata Litario, with subsamples #737A and #737B providing broadly consistent results (Tables 1 and S5). In the first instance, these AAR data, unlike those of #738 and #739, do not exhibit any signs that the dentine has experienced major diagenetic alterations. In comparison, the two subsamples from tooth #852 provide contrasting results. The extremely high value of Alanine measured in subsample A (in red in Table S5) and anomalous D/L values (e.g., Csapò et al., 1998) suggests significant diagenetic alteration of the dentine, raising doubts about the reliability of this AAR age. Moreover, some amino acids show anomalously high percentage values with respect to the total amino acid content of subsample A (i.e., Alanine = ca. 40%; Aspartic acid = ca. 13%). These high percentages are typical of younger samples (ca. 60-70 ka), thus indicating that the results of this subsample should be treated with caution. Consequently, this subsample is not considered further in the final discussion. In contrast, the data obtained for subsample B are within usual standards (e.g., Laabs and Kaufman, 2003; Kosnik and Kaufman, 2008), and the resulting age of 261 ka can be regarded as methodologically reliable.

4.3 Luminescence dating of sediments

The measured grains produce weak TT-OSL signals, with approximately 76-85% of grains yielding no detectable luminescence (i.e. T_n signal <3 × signal background; Table S9) and a further 9-14% displaying T_n signals with large associated errors of >30% (Table S9). The proportion of measured grains per sample that pass the single-grain TT-OSL SAR rejection criteria is generally very low, between 0.8 and 2.4% (Table S9). These TT-OSL signals of these grains are fast-decaying and generally decrease by ~90% within the first 0.32 s of stimulation (e.g., Figure 3B). The single-grain TT-OSL dose-response curves are all well-represented by a single saturating exponential function and display continued signal growth at high doses (>10^3 Gy) (Figure 3B).

All pIR-IRSL$_{225}$ signals are bright and fast decaying, with the signals decreasing by >90% in the first 20 s of stimulation. Figure 3C shows an example of a multi-grain pIR-ISL$_{225}$ decay curve and corresponding dose-response curve for sample CL16-4. The dose response curves are optimally fitted using an exponential plus linear function. For all samples the D_e estimate was calculated from the non-saturated portion of the dose response curve (D_e values = ~1200 Gy). Assessments of anomalous fading were performed to investigate the potential for long-term athermal loss of the K-feldspar pIR-IRSL$_{225}$ signal over burial timescales. These results are shown in Table S12 and discussed in section 5.5 of the Supplementary Information.

The single-grain TT-OSL D_e distributions obtained do not display typical partially bleached or syn-depositionally mixed patterns (i.e., there is a general absence of distinct leading-edges of low D_e values or elongated tails of higher D_e values; see example shown in Figure 3D). They are characterised by low to moderate scatter, with overdispersion values between 20% and 38% (Table S13), and with D_e values that are mostly randomly spread around the mean (Figure S3). Additionally, the weighted skewness scores indicate that none of the samples are significantly positively skewed according to the criterion outlined by Arnold and Roberts (2009) (Table S13).

Similarly, all pIR-IRSL$_{225}$ D_e distributions display low scatter, with overdispersion values ranging from 0% to 19% (example shown in Figure 3E). None of the pIR-IRSL$_{225}$ D_e datasets display the typical asymmetric spread associated with partially bleached grain populations, as shown by the weighted skewness scores (Figure S4 and Table S14). These indicators suggest the pIR-IRSL$_{225}$ signals of all samples were well-bleached at deposition and do not contain syn-depositionally mixed grain populations, consistent with the single-grain TT-OSL results. Consequently, the central age model (CAM) of Galbraith et al. (1999) has been used to calculate mean D_e values for both the TT-OSL and pIR-IRSL datasets. This choice of age model is also supported by the L_{max} scores obtained for the different age models, which indicate the CAM is statistically favoured over the 3-parameter and 4-parameter minimum age models (MAM-3 and MAM-4 in Table S13 and Table S14) in all instances.

>Figure 3<

Table 2 shows the final TT-OSL and pIR-IRSL$_{225}$ ages obtained in this study. All of the paired luminescence dating ages are in agreement at 1σ, though the TT-OSL ages are systematically younger than the pIR-IRSL$_{225}$ ages by 1-9%. While there is possible evidence of a minor stratigraphic age inversion for sample CL16-3, this is not statistically significant as the surrounding samples all produce ages in agreement at 1σ. No apparent age-depth trend is observed throughout the stratigraphy, suggesting that sediment deposition may have occurred over a timespan that cannot be resolved beyond the existing age uncertainties. The luminescence ages are mostly centred around MIS-11 (374-424 ka; Lisiecki and Raymo, 2005).

>*Table 2*<

4.4 U-series dating of speleothems

Sample SC118-A exhibits a very low ^{238}U content (64 ppb) but it is within the range of other dated speleothems from the Atapuerca karstic system (e.g., Martínez-Pillado et al., 2014). In contrast, the other four samples have high Uranium contents (250-400 ppb) compared with the values usually reported for speleothems (<200 ppb, Eggins et al., 2005). The relatively high ^{230}Th / ^{232}Th ratio of all the carbonate samples indicates that there is no significant contamination of detrital thorium. Consequently, the corresponding correction does not change the final ages beyond their existing uncertainty ranges (age deviation is <3 ka).

Speleothem SC118-A (LU2) covering the sediment infill sequence of Cata Litario pit yields a U-series age of 200 ± 4 ka (Table 3), placing its formation during MIS-7. This capping speleothem provides a minimum age constraint for the underlying fossiliferous levels.

The speleothem fragments embedded in LU6 (SC118-B and SCI23-A) provide ages of 318 ± 5 ka and 284 ± 4 ka (Table 3). While SC118-B is a horizontal flowstone fragment, SCI23-A has some vertical development, indicating a phase of speleothem formation in the cavity during MIS-9 that probably evolved to dripping forms within MIS-8. The two speleothem fragments from LU5 provide very scattered ages. The flowstone fragment SCI23-B yields an age of 310 ± 8 ka (Table 3), which could match with the formation episode of fragment SCI18-B from LU6. In comparison, stalagmite SCI23-C grew between 444 ± 19 and 433 ± 15 ka (Table 3), overlapping with the oldest chronologies obtained by luminescence dating for the host sediment deposits of LU5 (see Table 2).

None of these speleothem fragments (SC118-B, SCI23-A, SCI23-B, SCI23-C) are in their original position but fragmented, altered and re-incorporated into these lithostratigraphic units (Fig. S2). Therefore, the scattered U-series ages for these speleothems could reflect a preceding erosional event in Sala de los Cíclopes that caused the remobilization (or partial displacement) of the previous endokarst infilling and the fragmentation of the developed speleothems. Alternatively, these speleothem fragments may have been locally reworked within the Cata Litario sedimentary sequence (or local vicinity) by post-depositional mixing processes, including being translocated vertically by plastic deformation and slumping of the host LUs 6, 5 and 4 clay deposits.

>Table 3<

5. Discussion

5.1. Galería de las Estatuas

The various combined U-series ages calculated for the two teeth from LU4 range from 87 ± 9 ka to 117 ± 13 ka depending on the conditions considered (e.g., age calculation program, uranium uptake model). These results are consistent with the previous OSL and U-series/ESR dating results available for the same unit, which are between 92 ± 6 ka and 112 ± 7 ka (Demuro et al., 2019a; Moreno et al., 2022; Fig. 2). In particular, our results compare well with the US-ESR ages of 95 ± 33 and 92 ± 6 ka independently obtained by Moreno et al. (2022) on two teeth from the same unit, although the latter should be considered with relative caution from a methodological viewpoint given (i) the relatively low goodness-of-fit achieved for the ESR DRC (r^2 <0.96), (ii) a D_{max}/D_E ratio exceeding by far the range (5-10) recommended by Duval and Grün (2016), (iii) and the absence of directly associated U-series data for some dental tissues.

To sum up, our dating results agree with the existing data set available for LU-4 from GE-I. The consistent numerical ages obtained from three independent studies (Demuro et al., 2019a; Moreno et al., 2022; this work), confirm the reliability and robustness of the existing chronostratigraphic constraints for the GE-I pit sequence, with units LU1 to 4 being deposited during MIS-5.

5.2. Cata Litario (Sala de los Cíclopes)

<u>5.2.1. Comparing the luminescence and U-series ages on sediment and carbonates</u>

This study provides the first set of ages for the Cata Litario pit at Sala de los Cíclopes. All luminescence ages are in agreement with each other at 1σ and suggest that the sampled sediment entered the cavity around MIS-11 (Figure 2; Table 2). These luminescence ages are compatible with the U-series age of 200 ± 4 ka obtained for sample (SCI18-A) from the speleothem capping the sequence (LU2), which post-dates the sediment deposition. The U-series ages obtained for the fragmented stalagmite within LU6 indicate a relatively stable dripping phase between 444 ± 19 and 433 ± 15 ka, suggesting its formation was coeval with, or slightly preceded, the entry of sediment into the cavity. All the other remobilised flowstone fragments collected from LUs 6 and 5 are considerably younger (between 318 ± 5 and 284 ± 8 ka) than the enclosing sediment, and have very rounded edges, which may indicate possible reworking of the sediment within the closed cavity prior to its deposition at Cata Litario. As an alternative (but non-exclusive) hypothesis, their position could also be the result of some post-depositional sediment disturbance at the site (including vertical translocation of broken speleothems), localised sediment slumping or plastic deformation of the clay-rich host deposits sometime between MIS-11 (age of sediment deposition) and MIS-7 (age of capping speleothem).

<u>5.2.2. Comparing U-series/ESR and AAR ages on fossils</u>

Non-overlapping U-Series/ESR and AAR ages of 217 ± 22 to 304 ± 33 ka and 378 ± 14 ka, respectively, were obtained from tooth #737 collected from Cata Litario level LU5. The reason for such a discrepancy requires a closer look at the available data. On the one hand, while dentine from #737 shows some U-leaching, this appears to have limited impact on the combined U-series/ESR age. The various calculations performed with different uranium uptake models return ages within 1σ error (Table 1) and are systematically younger than the AAR age. Nevertheless, since initial combined U-series/ESR age calculations had to be performed by considering the dentine as a closed system (p parameter in dentine fixed to -1), we acknowledge that the resultant ages are probably of lower reliability and robustness compared to #852. In comparison, the AAR data do not show any unusual contents or ratios that would indicate that the dentine has experienced major diagenetic alterations (Table S5). However, it is worth noting that the apparent U-series age of >500 ka obtained for the same dental tissue suggests otherwise (Table S3) and implies a significant uranium leaching overprint. Indeed, uranium uptake in fossils is usually regarded as a reliable proxy for diagenetic alteration (Kohn et al., 1999). Thus, we cannot discard the possibility that the dentine in sample #737 has experienced taphonomic or diagenetic alteration, which is consistent with field observations and especially with the tooth being located in close proximity to (directly below) the extensive and well-developed LU2 speleothem formation (Fig. S2B). Consequently, the corresponding AAR results for #737 should be treated with some caution. Interestingly, the possible correlations (or lack thereof) between U-series and AAR ages in dentine has never been explored to our knowledge. Additionally, heterogeneous spatial distribution of amino acids may also occur within a given material, such as shells (e.g., Brigham, 1983; Hearty et al., 1986; Carroll et al., 2003) or dental tissues (Torres et al., 2000). In this regard, Sejrup and Haugen (1994) indicate that differences in D/L values between the inner part of the sample and the outer can be produced by rapid and early degradation of the protein, possibly due to microbiological activity. We therefore cannot exclude the possibility that we may have sampled in a domain of the dentine that was not suitable for AAR dating. New AAR experiments are being carried out on these teeth in order to evaluate the spatial variability of the amino acid ratios within a given dental tissue.

Tooth #852, on the contrary, yields consistent ages of 258 ± 21 to 287 ± 23 ka using the two direct dating techniques (U-series/ESR and AAR (sample B), Table 1). These replicate ages are within error of each other, even after considering different uranium uptake models or post-Rn disequilibrium in dental tissues. They overlap with the U-series/ESR age range of 217 ± 22 to 304 ± 33 ka obtained for sample #737. Like the luminescence ages on the sediment, these direct ages on the fossils are compatible with the minimum age constraint of 200 ± 4 ka obtained on the overlying *in situ* speleothem of LU2.

To sum up, the combined U-series/ESR and AAR age discrepancies obtained for #737 could partly, or wholly, be explained by several methodological reasons. We therefore acknowledge that these methodological limitations may have resulted in questionable ages for tooth #737 compared to #852. Despite the two teeth from Cata Litario returning consistent U-series/ESR age ranges (Table 1), it may be reasonably considered that #852 provides more reliable chronological constraint for the fossils from LU5 from a methodological perspective. As such, the results derived from #737 are not considered further for the chronostratigraphic interpretation of the site.

5.2.3. Integrating all dating results

Despite both the luminescence dating results on one side, and the combined U-series/ESR and AAR dating results on the other, being chronostratigraphically consistent with the minimum age constraint provided by the uppermost LU2 speleothem, they nevertheless differ from each other by >100 ka (389-444 ka vs 256-287 ka), suggesting either the existence of a methodological bias, or that the fossil and host sediment may not be coeval. From a methodological perspective, dating carnivore teeth using U-series/ESR is especially challenging as the tooth structure (with a sharp morphology adapted to cut muscles and tendons) and the limited enamel thickness usually make them less suitable than herbivore teeth. In particular, this complicates the sample preparation procedure and the extraction and cleaning of the enamel layer. Dentine typically shows uranium concentrations of several orders of magnitude higher than in enamel (e.g., Table S3; Grün and Taylor, 1996), and any slight contamination may potentially significantly impact U-series data measured in the enamel and the resulting combined U-series/ESR age (e.g., Arsuaga et al., 2014; Duval et al., 2018). This potential issue may be reasonably discarded here given the relatively low uranium concentrations measured in the enamel samples (<1.5 ppm; Table S3). For example, these values are much lower than the 4.6 ppm measured in the enamel of a bear tooth from the nearby Sima de los Huesos site (Arsuaga et al., 2014), and for which dentine contamination was suspected. The overall uncertainty associated with the uranium uptake in the dental tissue of #852 may be estimated as being about 30 ka, depending on the model selected and whether a post-Rn disequilibrium in the U-238 decay chain is considered. However, on its own, this relative uncertainty of 11-12 % on the calculated U-series/ESR age cannot explain the apparent discrepancy with the luminescence results.

We have also evaluated the impact of the existing uncertainty associated with the gamma dose rate evaluation of #852, given that it was not possible to perform an *in situ* evaluation at the exact location of the tooth (unlike for #737; see full details in Supplementary Information; Fig. S2). An additional calculation based on the use of the raw sediment attached to the tooth for the determination of both the beta and gamma dose rate components returns a US-ESR age of 219 ± 21 ka, i.e., 37 ka lower than the initial estimate of 256 ± 24 ka (Table 1) and thus even more inconsistent compared to the luminescence dating results. While the accuracy of this alternative age estimate may be reasonably questioned since the sediment measured in the laboratory is unlikely to capture the real spatial heterogeneity of the natural radioactivity surrounding the tooth, this sensitivity test at least shows that the uncertainty on the gamma dose rate is unlikely to be the main cause of the age discrepancy between the U-series/ESR and luminescence ages. Based on the evidence discussed above, we can reasonably consider that this discrepancy is unlikely to be methodological, which is also supported by previous dating comparisons showing good agreement between these methods, including at other Atapuerca sites (Demuro et al., 2014; Ollé et al., 2016; Daura et al., 2015, 2017; Hocknull et al., 2020; Arnold et al., 2015, this volume; Stinchcomb et al., 2023).

The most parsimonious way to reconcile these results would be to consider that the age differences might simply result from asynchrony between the sedimentary fill and the fossiliferous deposit. This asynchrony may be due to either reworking of the sediment within the closed cavity prior to its deposition at Cata Litario and/or because of vertical translocation by post-depositional sediment disturbance. In the first scenario, it is assumed that the speleothem fragments and bear fossils may have been collected and transported from the floor in most elevated areas of the Sala de los Cíclopes during remobilisation of sediments towards the more depressed area of the cave (Cata Litario), as proposed by Aranburu et al. (2007). This hypothesis is potentially supported by the presence of horizontally arranged marls fragments from LU8 within LU6 (Fig. 2, S2D), the presence of red breccia clasts in LU4 and a complete red breccia level in LU3, and the high degree of erosion and corrosion of the external surface of speleothem fragments in LU6 and LU5 (Fig. 2F). The presence of sediment remnants, mostly fluvial sands and silts, and colluvial red-matrix breccia, are also observable as patches on the walls and ceiling of the Sala de los Cíclopes chamber, which indicate that complex erosive events took place after the original deposition of these sediments. Under this hypothesis, one could deduce the occurrence of a low energy flooding event in the cave by surface water inflow that remobilised the sediment remnants from the patches of roofs, walls and floors, and resedimented them together with the surface material that has washed down to Cata Litario. As the ages of all the embedded clasts, both fossils and speleothems, are in the range of 258 ± 21 and 444 ± 19 ka, and the capping *in situ* flowstone has 200 ± 4 ka, it could be assumed that such a remobilisation event occurred sometime between 284 ± 4.5 ka (age of the youngest exact age obtained, from speleothem SCI23-A) and 200 ± 4 ka (age of the capping flowstone), during MIS8 and/or MIS7. However, if this hypothesis were to be confirmed, then the ages resulting from both trapped charge dating methods (i.e., luminescence and combined U-series/ESR) should be treated with caution given that it would be impossible to properly assess the evolution of the environment dose rates throughout the full burial history in different parts of the cave system.

In the second alternative (but non-exclusive) scenario, vertical trampling downwards through the profile by localised post-depositional mixing of sediments, fossils and speleothem fragments preserved at the site may have occurred (i.e. because of post-depositional mixing and trampling by bears or because the bear remains are derived from hibernation beds that were dug into the original sediment profile, and exacerbated by plastic deformation and sediment slumping of the host clay deposits). This hypothesis is supported by the single-grain TT-OSL D_e datasets, which exhibit only minor to moderate scatter and do not provide clear evidence of syn-depositionally mixed grain populations that would otherwise be apparent if there were protracted and progressive re-transportation of the sediment within the karst system.

In some areas of the site, such as the eastern profile, the upper units (LU3, LU4 and LU5) are not well preserved and become thinner, with diffuse contacts between them, while to the west their integrity is better preserved and the contacts between them become clearer. This difference in preservation may be due to the proximity of the site to the east wall of the cave, as well as the presence of the speleothem in this profile, which has clearly carbonated the underlying sediments by water infiltration. The action of a more intense activity produced by bears in this eastern sector can also be considered, as a large number of bear bones can be seen at shallow depths. In general, for the whole pit, present-day evidence in favour of bear hibernation nests is scarce, but we cannot rule out their presence in the past. The preserved bear fossils do not show any anatomical connection and are fragmented and randomly distributed through LUs 6 and 5 (including being attached to the base of the LU2 flowstone), which implies some degree of mixing or mobilisation. However, there is no evidence of sediment caking due to bear nests or semi-circular hibernation structures, which are usually preserved even if they are refilled lately (i.e., those preserved in Galería Baja or in Sala de las Oseras). It is possible that at Cata Litario these structures have been erased due to trampling and the action of other later bears in the eastern sector of the site, where the stratigraphic units become more chaotic and show post-depositional alterations.

The LU5 fossil and speleothem samples dated in this study are all found at depths that range from 55 to 92 cm below the flowstone forming LU2. However, the surface is very irregular, the unit boundaries change depth quite significantly across a short distance of <1m, and trampling and digging influences may have extended sediment perturbation down a further 10-20 cm, so we cannot discount the possibility that the present-day depth for fossils and clasts in this LU are not reflective of their original or long-term depths. The LU6 speleothem fragments, on the other hand, are found at depths up to 112 cm below the flowstone forming LU2, while several bear bone fragments can be observed in the site profiles at depths of almost 1.5 m. In the southwest profile of Cata Litario, the lithological units show clear developments and contacts, and there is no trace of any hibernation structures and no geological evidence of vertical remobilisation of the sediments. For the rounded speleothem fragments and bear bones in this profile, at depths > 1m with an unaltered sequence above, we cannot confidently attribute their presence to the action of bears considering their present-day configuration, as they are too deep to have been excavated by a bear for its hibernation bed. Mean bear bed depths of 20 cm, and maximum depths of 40 cm, may be expected based on available data from different European caves sites for brown bear (*U. arctos*) and cave bear (*U. spelaeus*) nests (Fosse et al., 2004). Values up to 50 cm have been found for both *U. spelaeus* and *U. deningeri* cave bears beds (Torres, 2014). In several paleontological sites under study (not yet published), including the Sala de las Oseras, well-preserved bear hibernation dens have been measured and studied by some of the authors of the present work. All the structures yield vertical depths ranging between 20 and 30 cm, so it seems unlikely that the bears at Sala de los Cíclopes would have made hibernation dens nor disturbed the sediment by trampling at 1.5 metres deep. However, it should be borne in mind that the present-day depth beneath surface is only a maximum estimate of the true depth beneath the long-term average surface, and hence a fossil sample at a 1.5 m depth today was not always necessarily beneath the influence of bear beds in the past. It may be that there are multiple generations of bear remains at this site and those fossil remains preserved in the lower profile (1.5 m beneath surface) may have a different age to the samples dated in this study from closer to the surface. For LU6, two specific scenarios can therefore be postulated. The first would support the hypothesis of resedimentation of the Cata Litario sequence, during which the fossils and speleothems were embedded in the sediments during their transport. In the second case, the fossils could belong to older generations of bears and may have been deposited together with the LU6 sediment prior to the sedimentation of LU5. Direct dating of the LU6 fossils will be necessary to support or rule out these hypotheses.

The potential for complex post-depositional sediment mixing and trampling of speleothem fragments is difficult to assess in the absence of detailed taphonomic and sedimentology studies, particularly as the current excavation only covers a very limited lateral extent (2 m), and taking into account the general complex karst sedimentary dynamics (e.g., Duval et al., 2024). Given the lateral rapid changes in the geology of cave deposits, additional test pits in topographically higher places within Sala de los Cíclopes could provide additional information regarding the complex processes of deposition and erosion within this chamber. Additionally, a more detailed geological study of the Cata Litario levels must be undertaken to understand the formation of the sequence and the post-depositional processes that have taken place in the site in order to find a more secure explanation for the scattered U-series ages and the disparity between the direct ages on the teeth and the luminescence ages for the host sediment.

Conclusion

We provide new dating results using a multi-technique approach for two key sites of the Atapuerca karst complex, Galeria de las Estatuas and Sala de los Ciclopes. Most dating methods return consistent ages for Galeria de las Estatuas, enabling us to establish a relatively simple chronostratigraphy for the site. In contrast, the numerical ages obtained for Sala de los Ciclopes reveal a much more complex picture of site formation and post-depositional processes, suggesting that the fossils and host sediment may not be coeval. Further work is required to confirm the different hypotheses proposed here for explaining the apparent discrepancies between the luminescence and combined U-series/ESR ages. This study highlights that results obtained using a single dating method may not always reliably represent the age of a deposit or fossil as potential biases may naturally arise, particularly in complex sedimentary settings such as caves. A multi-technique dating approach that targets different materials is the most secure means of reconstructing reliable chronological frameworks, although it is also necessary to understand the geological factors that could have affected the dating materials, including the accumulation and taphonomic histories of fossils, and post-depositional and remobilisation processes affecting sediments.

Acknowledgements

The authors are especially grateful to María Jesús Alonso Escarza, Alicia Churruca Clemente and Javier Iglesias Cibanal, CENIEH, for technical support throughout the ESR analytical procedure, to Yolanda Sánchez Palencia for her help during the AAR samples preparation, and to Nohemi Sala Burgos for her help and support with the geological and stratigraphical information of the sites. We would also like to thank the work and effort of all the members of the excavation and research team of the Galería de las Estatuas and

Sala de los Cíclopes, which has allowed us to access and recover the samples. We are grateful for the comments provided by the anonymous reviewers and the Editor that have helped to improve this paper.

This work is part of Grant PID2021-123092NB-C22 funded by MCIN/AEI/ 10.13039/501100011033/'ERDF A way of making Europe' and research project PID2021-122355NB-C31, MCIN/AEI/10.13039/501100011033/ FEDER, UE (Spanish Ministerio de Ciencia e Innovación). The Spanish Ramón y Cajal fellowship RYC2018-025221-I awarded to MDu is funded by MCIN/AEI/ 10.13039/501100011033 and by 'ESF Investing in your future'. MDe was supported by Australian Research Council (ARC) Future Fellowship FT200100816 and ARC Discovery Early Career Researcher Award DE160100743, AGO is supported by a Ramón y Cajal fellowship (RYC2017-22558). Fieldwork in the Sierra de Atapuerca sites is funded by the Junta de Castilla y León and Fundación Atapuerca.

References

Aitken 1998. An Introduction to Optical Dating: The Dating of Quaternary Sediments by the Use of Photon-Stimulated Luminescence. Oxford University Press, Oxford, 267 p.

Aranburu, A., Ortega, A.I., Iriarte, E., Dorado, M., Valdeolmillos, A., Ruiz Zapata, MB., Arsuaga, J.L., 2007. Estratigrafía endorkárstica pleistocena de la Sierra de Atapuerca (Burgos): Datos geoambientales desde la Sala de los Cíclopes. Resúmenes XII Reunión Nacional de Cuaternario, 41-42.

Aranburu, A., Martínez-Pillado, V., García, F., Arsuaga, J. L., Alcázar de Velasco, A. Bonmatí, A., García, N., Gracia, F., Gómez, A., Lira, J., Lorenzo, C., Martínez, I., Ortega, A.I., Pablos, A., Pantoja, A., Quam, R., Sala, N., 2012. La variabilidad de los rellenos endokársticos de la Galería de Estatuas (Atapuerca, Burgos) y su caracterización paleoambiental. Avances de la Geomorfología en España, 397-400.

Arnold, L.J., Demuro, M., 2015. Insights into TT-OSL signal stability from single-grain analyses of known-age deposits at Atapuerca, Spain. Quaternary Geochronology 30B, 472-478.

Arnold, L.J., Demuro, M., Duval, M., Grün, R., Sanz, M., Costa, A.M., Araújo, A.C., Daura, J., Single-grain luminescence and combined U-series/ESR dating of the early Upper Palaeolithic Lagar Velho Rock Shelter. Quaternary Geochronology, submitted.

Arnold, L.J., Demuro, M., Navazo Ruiz, M., Benito-Calvo, A., Pérez-González, A., 2013. OSL dating of the Middle Palaeolithic Hotel California site, Sierra de Atapuerca, north-central Spain. Boreas 42, 285-305.

Arnold, L.J., Demuro, M., Navazo Ruiz, M., 2012b. Empirical insights into multi-grain averaging effects from 'pseudo' single-grain OSL measurements. Radiat. Meas., 47 (2012), pp. 652-658.

Arnold, L.J., Demuro, M., Parés, J.M., Arsuaga, J.L., Aranburu, A., Bermúdez de Castro, J.M., Carbonell, E., 2014. Luminescence dating and palaeomagnetic age constraint on hominins from Sima de los Huesos, Atapuerca, Spain. Journal of Human Evolution 67, 85-107.

Arnold, L.J., Demuro, M., Parés, J.M., Pérez-González, A., Arsuaga, J.L., Bermúdez de Castro, J.M., Carbonell, E., 2015. Evaluating the suitability of extended-range luminescence dating techniques over Early and Middle Pleistocene timescales: Published datasets and case studies from Atapuerca, Spain. Quaternary International 389, 167-190.

Arnold, L.J., Demuro, M., Power, R., Priya, Duval, M., Guilarte, V., Weij, R., Woodhead, J., White, L., Bourne, S., Reed, E.H., 2022. Examining sediment infill dynamics at Naracoorte cave megafauna sites using multiple luminescence dating signals. Quaternary Geochronology 70, 101301.

Arnold, L.J., Demuro, M., Spooner, N.A., Prideaux, G.J., McDowell, M., Camens, A.B., Reed, E.H., Paress, J.M., Arsuaga, J.L., Bermúdez de Castro, J.M., Carbonell, E., 2019. Single-grain TT-OSL bleaching characteristics: Insights from modern analogues and OSL dating comparisons. Quaternary Geochronology 49, 45-51.

Arnold, L.J., Duval, M., Falguères, C., Bahain, J.-J., Demuro, M., 2012a. Portable gamma spectrometry with cerium-doped lanthanum bromide scintillators: suitability assessments for luminescence and electron spin dating applications. Radiation Measurements 47, 6-18.

Arnold, L.J., Roberts, R.G., 2009. Stochastic modelling of multi-grain equivalent dose

(De) distributions: Implications for OSL dating of sediment mixtures. Quaternary Geochronology 4, 204-230.

Arsuaga, J.L., Carretero, J.-M., Lorenzo, C., Gómez-Olivencia, A., Pablos, A., Rodríguez, L., García-González, R., Bonmatí, A., Quam, R.M., Pantoja-Pérez, A., Martínez, I., Aranburu, A., Gracia-Téllez, A., Poza-Rey, E., Sala, N., García, N., Alcázar de Velasco, A., Cuenca-Bescós, G., Bermúdez de Castro, J.M., Carbonell, E., 2015. Postcranial morphology of the middle Pleistocene humans from Sima de los Huesos, Spain. Proceedings of the National Academy of Sciences of the United States of America, 112: 11524-11529.

Arsuaga, J.L., Martínez, I., Arnold, L.J., Aranburu, A., Gracia-Téllez, A., Sharp, W.D., Quam, R.M., Falguères, C., Pantoja-Pérez, A., Bischoff, J., Poza-Rey, E., Parés, J.M., Carretero, J.M., Demuro, M., Lorenzo, C., Sala, N., Martinón-Torres, M., García, N., Alcázar de Velasco, A., Cuenca-Bescós, G., Gómez-Olivencia, A., Moreno, D., Pablos, A., Shen, C.C., Rodríguez, L., Ortega, A.I., García, R., Bonmatí, A., Bermúdez de Castro, J.M., Carbonell, E., 2014. Neandertal roots: Cranial and chronological evidence from Sima de los Huesos. Science, 344 (6190): 1358-1363.

Arsuaga, J.L., Martínez, I., Gracia, A., Carretero, J.M., Lorenzo, C., García, N., Ortega, A.I., 1997. Sima de los Huesos (Sierra de Atapuerca, Spain). The Site. Journal of Human Evolution 33, 109-127.

Arsuaga, J.L., Martínez, I., Gracia, A., Carretero, J.M., Esquivel, A., García, N., Lorenzo, C., Quam, R.M., Aranburu, A., Sala, N., Trueva, J., 2024. How the Sima de los Huesos was won. The Anatomical Record, Special issue article 1–21.

Arsuaga, J.L., Gómez-Olivencia, A., Sala, N., Martínez-Pillado, V., Pablos, A., Bonmatí, A., Pantoja-Pérez, A., Lira-Garrido, J., Alcázar de Velasco, A., Ortega, A.I., Cuenca-Bescós, G., García, N., Aranburu, A., Ruiz-Zapata, B., Gil-García, M.J., Rodríguez-Alvarez, X.P., Ollé, A., Mosquera, M., 2017. Evidence of paleoecological changes and Mousterian occupations at the Galería de las Estatuas site, Sierra de Atapuerca, norther Iberian plateau, Spain. Quaternary Research 88, 345-367.

Bada J.L., Protsch, R., 1973. Racemization Reaction of Aspartic Acid and Its Use in Dating Fossil Bones, Proceedings National Academy of Science 70, 1331-1334.

Bergamín, J.F., Sánchez, F., Sánchez, N., Souto, J., Arsuaga, J.L., 1994. Primeros resultados de la prospección geofísica en la zona suroeste de la Cueva Mayor (Sima de los Huesos), Atapuerca (Burgos). Geoarqueología (Actas de la 2a Reunión Nacional de Geoarqueología). I.T.G.E.-AEQUA 449-456.

Brigham, J.K., 1983. Intrashell variation in amino acid concentrations and isoleucine epimerization ratios in fossil Hiatella arctica. Geology 11, 509-513.

Buylaert, J.P., Jain, M., Murray, A.S., Thomsen, K.J., Thiel, C., Sohbati, R., 2012. A robust feldspar luminescence dating method for Middle and Late Pleistocene sediments. Boreas 41, 435-451.

Carbonell, E., Bermúdez de Castro, J.M., Arsuaga, J.L., Díez, J.C., Rosas, A., Cuenca-Bescós, G., Sala, R., Mosquera, M., Rodríguez, X.P., 1995. Lower Pleistocene hominids and artefacts from Atapuerca-TD6 (Spain). Science 269, 826-830.

Carbonell, E., Bermúdez de Castro, J.M., Parés, J.M., Pérez-González, A., Cuenca-Bescós, G., Ollé, A., Mosquera, M., et al., 2008. The first hominin of Europe. Nature 452, 465-469.

Carbonell, E., Huguet, R., Cáceres, I., Lorenzo, C., Mosquera, M., Ollé, A., Rodríguez, X. P., Saladie, P., Vergès, J.M., García, P., Rosell, J., Vallverdú, J., Carretero, J.M., Navazo, M., Ortega, A.I., Martinón-Torres, M., Muro, J.I., Allúe, E., Aranburu, A., Canals, A., Carrancho, A., Castilla, M., Expósito, I., Fontanals, M., Francés-Negro, M., Galindo-Pellicena, M.A., García-Antón, M.D., García, N., Gracia, F., Gómez-Merino, G., García, R., Iriarte, E., de Lombera-Hermida, A., López-Polín, L., Lozano, M., van der Made, J., Martínez, I., Mateos, A., Pérez-Romero, A., Poza-Rey, E., Quam, R., Rodríguez, A., Rodríguez, J., Rodríguez, L., Santos, E., Terradillos, M., Bermúdez de Castro, J.M., Arsuaga, J.L., 2014. Sierra de Atapuerca archaeological sites. In: Sala, R., Carbonell, E., Bermúdez de Castro, J.M., Arsuaga, J.L. (Eds.), Pleistocene and Holocene Hunter-Gatherers in Iberia and the Gibraltar Strait: the Current Archaeological Record. Fundación Atapuerca - Universidad de Burgos, Servicio de publicaciones, pp. 534-560.

Carretero, J.M., Ortega, A.I., Juez, L., Pérez-González, A., Arsuaga, J.L., Pérez-Martínez, R., Ortega, M.C., 2008. A Late Pleistocene-Early Holocene archaeological sequence of Portalón de Cueva Mayor (Sierra de Atapuerca, Burgos, Spain). Munibe (Antropologia-Arkeologia) 59, 67-80.

Carroll, M., Kowalewski, M., Simões, M.G., Goodfriend, G.A., 2003. Quantitative estimates of time averaging in terebratulid brachiopod shell accumulations from a modern tropical shelf. Paleobiology 29, 381-402.

Cheng, H., Edwards, R.L., Shen, C.C., Polyak, V.J., Asmerom, Y., Woodheah, J., Hellstrom, J., Wang, Y., Kong, X., Spötl, C., Wang, X., Alexander Jr, E.C., 2013. Improvements in ^{230}Th dating, ^{230}Th and ^{234}U half-life values, and U-Th isotopic measurements by multi-collector inductively coupled plasma mass spectrometry. Earth and Planetary Science Letters, 371-372: 82-91.

Csapò, J., Csapó-Kiss, Z., Csapó Jr., J., 1998. Use of amino acids for age determination in archaeometry. Trends in Analytical Chemistry 17, 140-148.

Daura, J., Sanz, M., Allué, E., Vaquero, M., López-García, J.M., Sánchez-Marco, A., Domènech, R., Martinell, J., Carrión, J.S., Ortiz, J.E., Torres, T., Arnold, L.J., Benson, A., Hoffmann, D.L., Skinner, A.R., Julià, R., 2017. Palaeoenvironments of the last Neanderthals in SW Europe (MIS 3): Cova del Coll Verdaguer (Barcelona, NE of Iberian Peninsula). Quaternary Science Reviews 177, 34-56.

Daura, J., Sanz, M., Julià, R., García-Fernández, D., Fornós, J.J., Vaquero, M., Allué, E., López-García, J.M., Blain, H.A., Ortiz, J.E., Torres, T., Albert, R.M., Rodríguez-Cintas, À., Sánchez-Marco, A., Cerdeño, E., Skinner, A.R., Asmeron, Y., Polyak, V.J., Garcés, M., Arnold, L.J., Demuro, M., Pike, A.W.G., Euba, I., Rodríguez, R.F., Yagüe, A., Villaescusa, L., Gómez, S., Rubio, A., Pedro, M., Fullola, J. M., Zilhão, J., 2015. Cova del Rinoceront (Castelldefels, Barcelona): a terrestrial record for the Last Interglacial period (MIS 5) in the Mediterranean coast of the Iberian Peninsula. Quaternary Science reviews 114, 203-227.

Demuro, M., Arnold, L.J., Aranburu, A., Gómez-Olivencia, A., Arsuaga, J.L., 2019a. Single-grain OSL dating of the Middle Palaeolithic site of Galería de las Estatuas, Atapuerca (Burgos, Spain). Quaternary Geochronology 49, 254-261.

Demuro, M., Arnold, L.J., Aranburu, A., Sala, N., Arsuaga, J.L., 2019b. New bracketing luminescence ages constrain the Sima de los Huesos hominin fossils (Atapuerca, Spain) to MIS 12. Journal of Human Evolution 131, 76-95.

Demuro, M., Arnold, L., Parés, J.M., Aranburu, A., Huguet, R., Valverdú, J., Arsuaga, J.L., Bermúdez de Castro, J.M., Carbonell, E., 2022. Extended-range luminescence chronologies for the Middle Pleistocene units at the Sima del Elefante archaeological site (Sierra de Atapuerca, Burgos, Spain). Quaternary Geochronology 71, 101318.

Demuro, M., Arnold, L.J., Parés, J.M., Pérez-González, A., Ortega, A.I., Arsuaga, J.L., Bermúdez de Castro, J.M., Carbonell, E., 2014. New luminescence ages for the Galería Complex archaeological site: resolving chronological uncertainties on the Acheulean record of the Sierra de Atapuerca, northern Spain. PLoS One 9, e110169.

Douville, E., Salle, E., Frank, N., Eisele, M., Pons-Branchu, E., Ayrault, S., 2010. Rapid and accurate U-Th dating of ancient carbonates using inductively coupled plasma-quadrupole mass spectrometry. Chemical Geology 272, 1-11.

Duval, M., 2015. Electron Spin Resonance (ESR) Dating of Fossil Tooth Enamel. Encyclopedia of Scientific Dating Methods. W. J. Rink and J. W. Thompson, Springer Netherlands: pp 239-246.

Duval, M., Arnold, L.J., 2013. Field gamma dose-rate assessment in natural sedimentary contexts using LaBr3(Ce) and NaI(Tl) probes: A comparison between the "threshold" and "windows" techniques. Applied Radiation and Isotopes 74, 36-45.

Duval, M., Arnold, L.J., Bahain, J.-J., Parés, J.M., Demuro, M., Falguères, C., Shao, Q., (...), Arzarello, M., 2024. Re-examining the earliest evidence of human presence in western Europe: New dating results from Pirro Nord (Italy). Quaternary Geochronology 82, 101519.

Duval M., Fang F., Suraprasit K., Jaeger J.-J., Benammi M., Chaimanee Y., Iglesias Cibanal J., Grün R., 2019. Direct ESR dating of the late Middle Pleistocene vertebrate assemblage from Khok Sung locality, Nakhon Ratchasima Province, Northeast Thailand. Palaeontologia Electronica 22.3.69, pp. 1-25.

Duval, M., Grün, R., 2016. Are published ESR dose assessments on fossil tooth enamel reliable? Quaternary Geochronology 31, 19-27.

Duval, M., Grün, R., Parés, J.P., Martín-Francés, L., Campaña, I., Rosell, J., Shao, Q., Arsuaga, J.L., Carbonell, E., Bermúdez de Castro J.M., 2018. The first direct ESR dating of a hominin tooth from Atapuerca Gran Dolina TD-6 (Spain) supports the antiquity of Homo antecessor. Quaternary Geochronology 47, 120-137.

Edwards, R.L., Chen, J.H., Wasserburg, G.J., 1987. 238U, 234U, 230Th, 232Th systematic and the precise measurement of time over the past 500,000 years. Earth and Planetary Science Letters 81, 175-192.

Eggins, S.M., Grün, R., Mcculloch, M.T., Pike, A.W.G., Chappell, J., Kinsley, L., Mortimer, G., Shelley, M., Murray-Wallace, C.V., Spotl, C., Taylor, L., 2005. In situ U-series dating by laser-ablation multi-collector ICPMS: new prospects for Quaternary geochronology. Quaternary Science Reviews 24, 2523-2538.

Fosse, P., Besson, J.P., Laborde, H., Thomas-Cantie, F., Cazenave, G., Delmasure, M.C., Lévêque, T., Laudet, F., Quilès. J., 2004. Denning behaviour of 'modern' brown bear (*U. arctos* L.) in caves: biological and paleontological considerations from French Pyrenean sites, in: M. Philippe, A. Argant, J. Argant (Eds.), 9th International Cave Bear Symposium, Cahiers scientifiques, hors série No. 2, Lyons, 171-182.

Galbraith, R.F., Roberts, R.G., Laslett, G.M., Yoshida, H., Olley, J.M., 1999. Optical dating of single and multiple grains of quartz from Jinmium Rock Shelter, Northern Australia: Part I, experimental design and statistical models. Archaeometry 41, 339-364.

García, N., Arsuaga, J.L., Torres, T., 1997. The carnivore remains from the Sima de los Huesos Middle Pleistocene site (Sierra de Atapuerca, Spain). Journal of Human Evolution 33, 155-174.

Goodfriend, G.A., Flessa, K.W., Hare, P.H., 1997. Variation in amino acid epimerization rates and amino acid composition among shell layers in the bivalve Chione from the Gulf of California. Geochimica et Cosmochimica Acta 61, 1487-1493.

Grün, R., 2000. An alternative model for open system U-series/ESR age calculations: (closed system U-series)-ESR, CSUS-ESR. Ancient TL 18(1): 1-4.

Grün, R., 2009. The DATA program for the calculation of ESR age estimates on tooth enamel. Quaternary Geochronology 4(3): 231-232.

Grün, R., Schwarcz, H.P. and Chadam, J., 1988. ESR dating of tooth enamel: Coupled correction for U-uptake and U-series disequilibrium. International Journal of Radiation Applications and Instrumentation. Part D. Nuclear Tracks and Radiation Measurements 14(1-2), 237-241.

Grün, R., Taylor, L., 1996. Uranium and Thorium in the Constituents of Fossil Teeth. Ancient TL 14(1): 21-25.

Guérin, G., Mercier, M., Adamiec, G., 2011. Dose-rate conversion factors: update. Ancient TL 29, 5-8.

Hearty, P.J., Miller, G.H., Stearns, C.E., Szabo, B.J., 1986. Aminostratigraphy of Quaternary shorelines in the Mediterranean Basin. Geological Society of America Bulletin, 97: 850-858.

Hocknull, S.A., Lewis, R., Arnold, L.J., Pietsch, T., Joannes-Boyau, R., Price, G.J., Moss, P., Wood, R., Dosseto, A., Louys, J., Olley, J., Lawrence, R.A., 2020. Extinction of eastern Sahul megafauna coincides with sustained environmental deterioration. Nature Communications 11, 2250.

Huntley, D.J., Baril, M.R., 1997. The K content of the K-feldspars being measured in optical dating or in thermoluminescence dating. Ancient TL 15, 11-13.

Huntley, D.J., Hancock, R.G.V., 2001. The Rb contents of the K-feldspar grains being measured in optical dating. Ancient TL 19, 43-46.

Kohn, M., Schoeninger, M.J., Barker, W., 1999. Altered states: Effects of diagenesis on fossil tooth chemistry. Geochimica et Cosmochimica Acta 63, 18, 2737-2747.

Lisiecki, L.E., Raymo, M.E., 2005. A Pliocene-Pleistocene stack of 57 globally distributed benthic $\delta^{18}O$ records. Paleoceanography 20, PA1003.

Martínez-Pillado, V., Aranburu, A., Arsuaga, J.L., Ruiz-Zapata, B., Gil-García, M.J., Stoll, H., Yusta, I., Iriarte, E., Carretero, J.M., Edwards, R.L., Cheng, H., 2014. Upper Pleistocene and Holocene palaeoenvironmental records in Cueva Mayor karst (Atapuerca, Spain) from different proxies: speleothem crystal fabrics, palynology, and archaeology. International Journal of Speleology 43, 1-14.

Marzin, E., 1990. Essai de normalisation du protocole d’analyse des taux de racémisation des acides aminés: applications a la datation d’ossements fossiles. Travaux du Lapmo (Laboratoire d’Antropologie et de Préhistoire des Pays de la Méditerranée Occidentale VIII, 167-178.

Moreno, D., Ortega, A.I., Falguères, C., Shao, Q., Tombret, O., Gómez-Olivencia, A., Aranburu, A., Trompier, F., Bermúdez de Castro, J.M., Carbonell, E., Arsuaga, J.L., 2022. ESR/U-series chronology of the Neanderthal occupation layers at Galería de las Estatuas (Sierra de Atapuerca, Spain). Quaternary Geochronology 72, 101342

Murray, A.S., Wintle, A., 2000. Luminescence dating of quartz using an improved single-aliquot regenerative-dose protocol. Radiation Measurements 32, 57-73.

Ollé, A., Vergès, J.M., Rodríguez, X.P., Cáceres, I., Angelucci, D.E., Vallverdú, J., Demuro, M., Arnold, L.J., Falguères, C., Bennàsar, M., López-García, J.M., Blain, H.A., Bañuls-Cardona, S., Burjachs, F., Expósito, I., López-Polín, L., López-Ortega, E., 2016. The Middle Pleistocene site of La Cansaladeta (Tarragona, Spain): Stratigraphic and archaeological succession. Quaternary International 393, 137-157.

Olivé, A., Ramírez, J.I., Ortega, L.I., Hernández, A., Alvaro, M., 1990. Mapa Geológico de España, E 1:50.000, Hoja n 201 (Belorado). IGME, Madrid.

Ortega Martínez, A.I., 2009. La evolución geomorfológica del karst de la Sierra de Atapuerca (Burgos) y su relación con los yacimientos pleistocenos. Tesis Doctoral. Universidad de Burgos, 624 p.

Ortega, A.I., Benito-Calvo, A., Pérez-González, A., Martín-Merino, M.A., Pérez-Martínez, R., Pares, J.M., Aramburu, A., Arsuaga, J.L., Bermúdez de Castro, J.L., Carbonell, E., 2013. Evolution of multilevel caves in the Sierra de Atapuerca (Burgos, Spain) and its relation to human occupation. Geomorphology 196, 122-137.

Ortega, A.I., Benito-Calvo, A., Pérez-González, A., Carbonell, E., Bermúdez de Castro, J.M., Arsuaga, J.L., 2014. Atapuerca Karst and its Palaeoanthropological Sites. En: Gutierrez, F., Gutierrez, M. (Eds.). Landscapes and Landforms of Spain, Word Geomorphological Landscapes. Springer, 101-111.

Ortega, A.I., Pérez-González, A., Martín-Merino, M.A., Carretero Díaz, J.M., Arsuaga, J.L., 2005. El Sistema Cueva Mayor-Cueva del Silo: Un estudio morfogenético del endokarst de la Sierra de Atapuerca (Burgos, España). In: Santonja, M., Pérez-González, A., Machado, M.J. (Eds.). Geoarqueología y Patrimonio en la Península Ibérica y el entorno Mediterráneo, 161-179. Adema. Soria.

Pablos, A., Gómez-Olivencia, A., Arsuaga, J.L., 2019. A Neandertal foot phalanx from the Galería de las Estatuas site (Sierra de Atapuerca, Spain). American Journal of

Physical Anthropology 168, 222-228.

Parés, J.M., Ortega, A.I., Benito-Calvo, A., Aranburu, A., Arsuaga, J.L., Bermúdez de Castro, J.M., Carbonell, E., 2016. Paleomagnetic constraints on the Atapuerca karst development (N Spain). En: Feinberg, J., Gao, Y., Alexander, E.C. Jr. (Eds.). Caves and Karst Across Time. Geological Society of America, Special Paper, 516: 285-300.

Parés, J.M., Pérez-González, A., Arsuaga, J.L., Bermúdez de Castro, J.M., Carbonell, E., Ortega, A.I., 2010. Characterizing the sedimentary history of cave deposits, using archaeomagnetism and roc magnetism, Atapuerca (Northern Spain). Archaeometry 52, 5, 882-898.

Pineda, A., Arce, J.M., 1997. Mapa Geologico de España, E 1:50.000, Hoja n 200 (Burgos). IGME, Madrid.

Prescott, J.R., Hutton, J.T., 1994. Cosmic ray contributions to dose rates for luminescence and ESR dating: large depths and long-term time variations. Radiation Measurements 23, 497-500.

Rodríguez, J., Burjachs, F., Cuenca-Bescós, G., García, N., Van der Made, J., Pérez González, A., Blain, H.A., et al., 2011. One million years of cultural evolution in a stable environment at Atapuerca (Burgos, Spain). Quaternary Science Reviews 30, 1396-1412.

Sejrup, H.P., Haugen, J.-E., 1994. Amino acid diagenesis in the marine bivalve Arctica islandica Linne´ from northwest European sites: only time and temperature? Journal of Quaternary Science 9, 301-309.

Shao, Q., Bahain, J.-J., Falguères, C., Dolo, J.-M. and Garcia, T., 2012. A new U-uptake model for combined ESR/U-series dating of tooth enamel. Quaternary Geochronology 10(0): 406-411.

Shao, Q., Bahain, J.J., Dolo, J.M., Falguères, C., 2014. Monte Carlo approach to calculate US-ESR age and age uncertainty for tooth enamel. Quaternary Geochronology 22, 99-106.

Shao, Q., Li, C.-H., Huang, M.-J., Liao, Z.-B., Arps, J., Huang, C.-Y., Chou, Y.-C., Kong, X.-G., 2019. Interactive programs of MC-ICPMS data processing for 230Th/U Geochronology. Quaternary Geochronology 51, 43-52.

Stevens, T., Buylaert, J.-P., Murray, A.S., 2009. Towards development of a broadly-applicable SAR TT-OSL dating protocol for quartz. Radiation Measurements 44, 639-645.

Stinchcomb, G.E., Quade, J., Levin, N.E., Iverson, N., Dunbar, N., McIntosh, W., Arnold, L.J., Demuro, M., Duval, M., Grün, R., Zhao, J.X., White, M., Hynek, S.A., Brown, F.H., Rogers, M.J., Semaw, S., 2023. Fluvial response to Quaternary Hydroclimate in Eastern Africa: Evidence from Gona, Afar, Ethiopia. Quaternary Science Reviews 309, 108083.

Torres, T. 2014. La historia del Oso de las Cavernas: vida y muerte de un animal desaparecido. Nuevas aportaciones de la excavación de la cueva de Amutxate (Aralar, Navarra). 162 pp. Laboratorio de Estratigrafía Biomolecular, Madrid.

Torres, T., Ortiz, J.E., Fernández, E., Arroyo-Pardo, E., Grün, R., Pérez-González, A., 2014. Aspartic acid racemization as a dating tool for dentine: A reality. Quaternary Geochronology 22, 43-56.

Torres, T., Ortiz J.E., García-Martínez, M.J., Llamas, F.J., Canoira, L., García de la Morena, M.A., 2000. Geochemical Evolution of Pleistocene Bears Dentine Amino Acids. Symposium on Biological Chirality (Szeged, Hungary).

Vernot, B., Zavala, E.I., Gómez-Olivencia, A., Jacobs, Z., Slon, V., Mafessoni, F., Romagné, F., Pearson, A., Petr, M., Sala, N., Pablos, A., Aranburu, A., de Castro, J.M. B., Carbonell, E., Li, B., Krajcarz, M.T., Krivoshapkin, A.I., Kolobova, K.A., Kozlikin, M.B., Shunkov, M.V., Derevianko, A.P., Viola, B., Grote, S., Essel, E., Herráez, D.L., Nagel, S., Nickel, B., Richter, J., Schmidt, A., Peter, B., Kelso, J., Roberts, R.G., Arsuaga, J.-L., Meyer, M., 2021. Unearthing Neanderthal population history using nuclear and mitochondrial DNA from cave sediments. Science 372, eabf1667.

Fig. 1- A) General location of the Sierra de Atapuerca sites (red star) in the Iberian Peninsula. B) Geological map of the Sierra de Atapuerca and the location of the Cueva Mayor cave system (modified from Pineda and Arce, 1997 and Olivé et al., 1990). C) Cross-sectional topographic profile of the Cueva Mayor-Cueva del Silo cave system (modified from Ortega Martínez, 2009). D) Planimetry of the Cueva Mayor-Cueva del Silo cave system, with the location of the Galería de las Estatuas and Sala de los Cíclopes (modified from Ortega et al., 2013).

Fig. 2- A) Detailed topographic profiles of Galería de las Estatuas and Sala de los Cíclopes, showing the location of the excavated test pits (Modified from Ortega Martínez, 2009 and Ortega et al., 2014). B) Stratigraphic logs and chronologies for the GE-I and Cata Litario (CL) pits and their correlation with Marine Isotope Stages (MIS). The combined U-series/ESR ages displayed here (light green stars) are: for GEI, the US-ESR age those obtained with USESR (Shao et al., 2014); for CL we are displaying the full possible range of US-ESR and CSUS ages considering equilibrium and disequilibrium in dental tissues (see Table 1). Except for the U-series ages on carbonates (2σ), all dating results are reported at 1σ. Global stack benthic δ^{18}O curve and MIS boundaries are taken from Lisiecki & Raymo (2005).

Fig. 3- (A) ESR dose response curves obtained for the four tooth enamel samples. Left DRC for each tooth: full dose range; Right DRC for ear tooth: zoom on the first irradiation points and the back extrapolation. For each sample, the two fittings displayed in this figure correspond to the evaluation of DE_4 and DE_5 (see Table S2 and section 3.4 of the Supplementary Information for explanation). (B) Representative single-grain TT-OSL decay and sensitivity-corrected dose response curves measured, example shown is from a grain of sample CL16-4. (C) Example of a representative multi-grain pIR-IRSL225 decay and sensitivity-corrected dose response curves measured from a multi-grain aliquot of sample CL16-4. (D) single-grain TT-OSL and (E) multi-grain pIR-IRSL225 De distributions obtained in this study and displayed as radial plots of sample CL16-4 from Cata Litario (Cueva Mayor, Atapuerca, Spain). Grey bars are centred on the CAM De.

Table captions:

Table 1- Overview of the Combined U-series/ESR and AAR dating results obtained on the four fossil teeth from GE-I and Cata Litario pits. All errors are 1σ. Individual AAR ages produced by the algorithm of Torres et al. (2014) do not have associated error. Mean AAR ages are shown with one standard deviation.

Table 2- Summary of single-grain TT-OSL and multi-grain pIR-IR225 dating results for the Cata Litario samples (Cueva Mayor-Cueva del Silo, Sierra de Atapuerca, Spain). Errors are 1σ.

Table 3- U-series dating results. The ages are shown with their associated 2σ uncertainties.

Figure 1

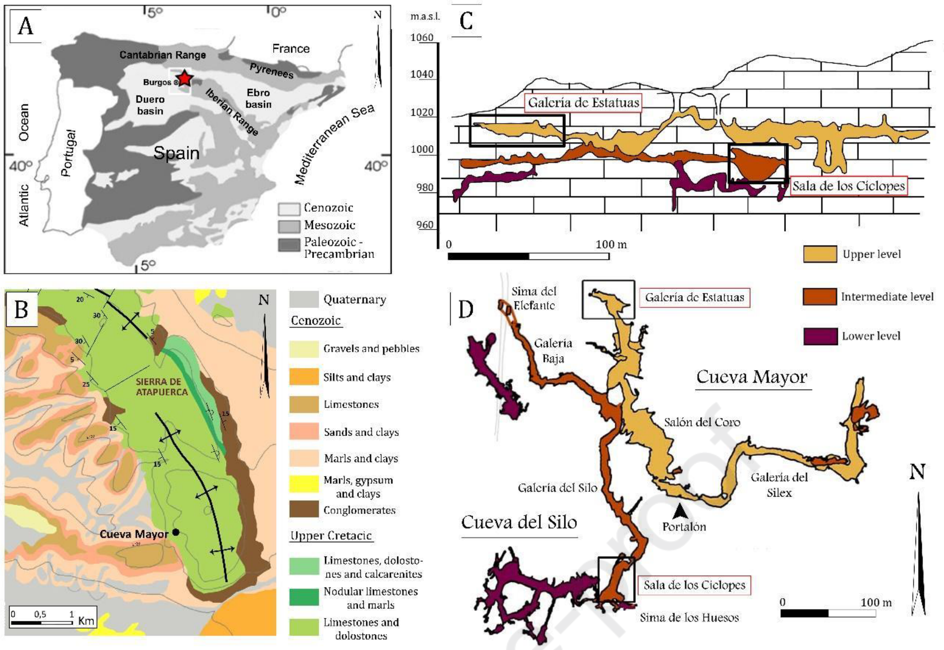
A
France
Cantabrian Range
Pyrenees
Burgos
Duero basin
Ebro basin
Iberian Range
Mediterranean Sea
Atlantic Ocean
Portugal
Spain
Cenozoic
Mesozoic
Paleozoic - Precambrian
B
SIERRA DE ATAPUERCA
Cueva Mayor
Km
Quaternary
Cenozoic
Gravels and pebbles
Silts and clays
Limestones
Sands and clays
Marls and clays
Marls, gypsum and clays
Conglomerates
Upper Cretacic
Limestones, dolostones and calcarenites
Nodular limestones and marls
Limestones and dolostones
C
m.a.s.l.
Galería de Estatuas
Sala de los Cíclopes
100 m
Upper level
Intermediate level
Lower level
D
Sima del Elefante
Galería Baja
Galería de Estatuas
Cueva Mayor
Salón del Coro
Galería del Silo
Galería del Silex
Portalón
Cueva del Silo
Sala de los Cíclopes
Sima de los Huesos
100 m

Figure 2

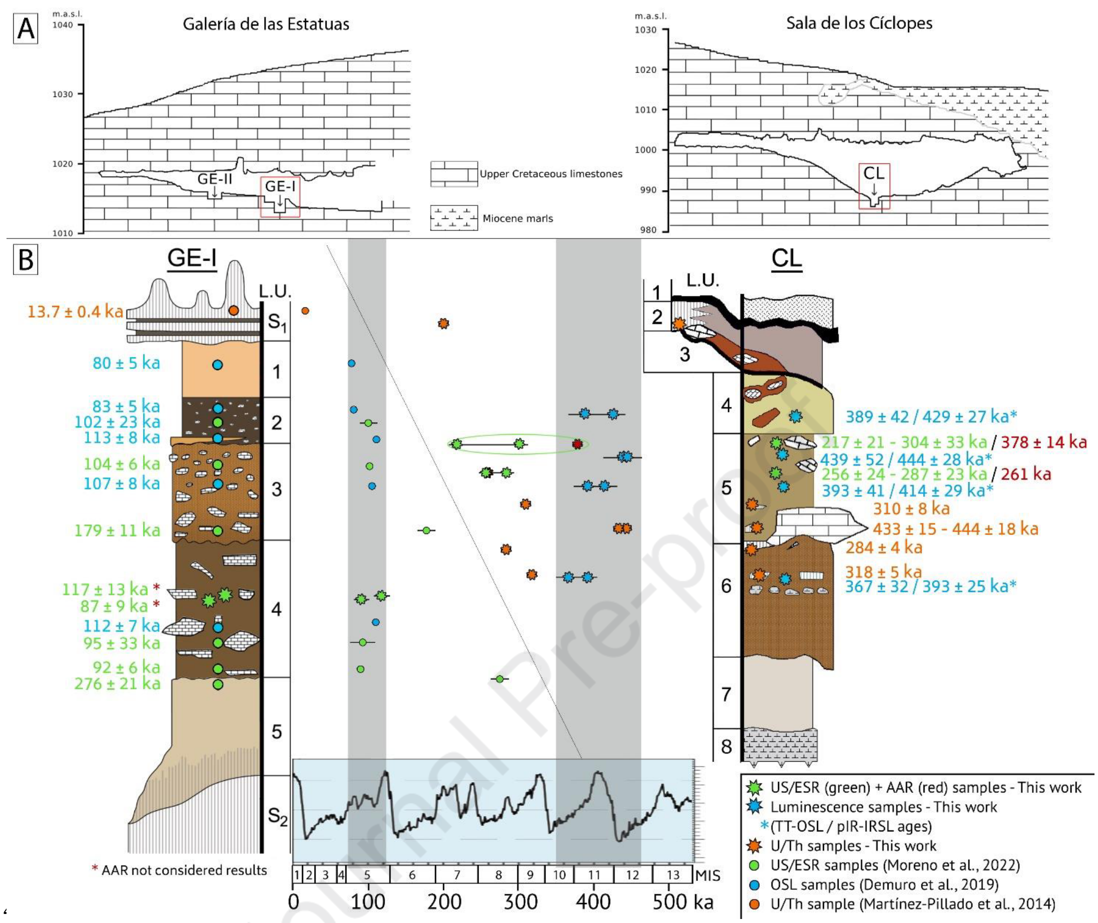
A
m.a.s.l.
Galería de las Estatuas
GE-II
GE-I
Upper Cretaceous limestones
Miocene marls
Sala de los Cíclopes
CL
B
GE-I
L.U.
13.7 ± 0.4 ka
80 ± 5 ka
83 ± 5 ka
102 ± 23 ka
113 ± 8 ka
104 ± 6 ka
107 ± 8 ka
179 ± 11 ka
117 ± 13 ka *
87 ± 9 ka *
112 ± 7 ka
95 ± 33 ka
92 ± 6 ka
276 ± 21 ka
* AAR not considered results
CL
389 ± 42 / 429 ± 27 ka*
217 ± 21 - 304 ± 33 ka / 378 ± 14 ka
439 ± 52 / 444 ± 28 ka*
256 ± 24 - 287 ± 23 ka / 261 ka
393 ± 41 / 414 ± 29 ka*
310 ± 8 ka
433 ± 15 - 444 ± 18 ka
284 ± 4 ka
318 ± 5 ka
367 ± 32 / 393 ± 25 ka*
MIS
0 100 200 300 400 500 ka
US/ESR (green) + AAR (red) samples - This work
Luminescence samples - This work
*(TT-OSL / pIR-IRSL ages)
U/Th samples - This work
US/ESR samples (Moreno et al., 2022)
OSL samples (Demuro et al., 2019)
U/Th sample (Martínez-Pillado et al., 2014)

Figure 3

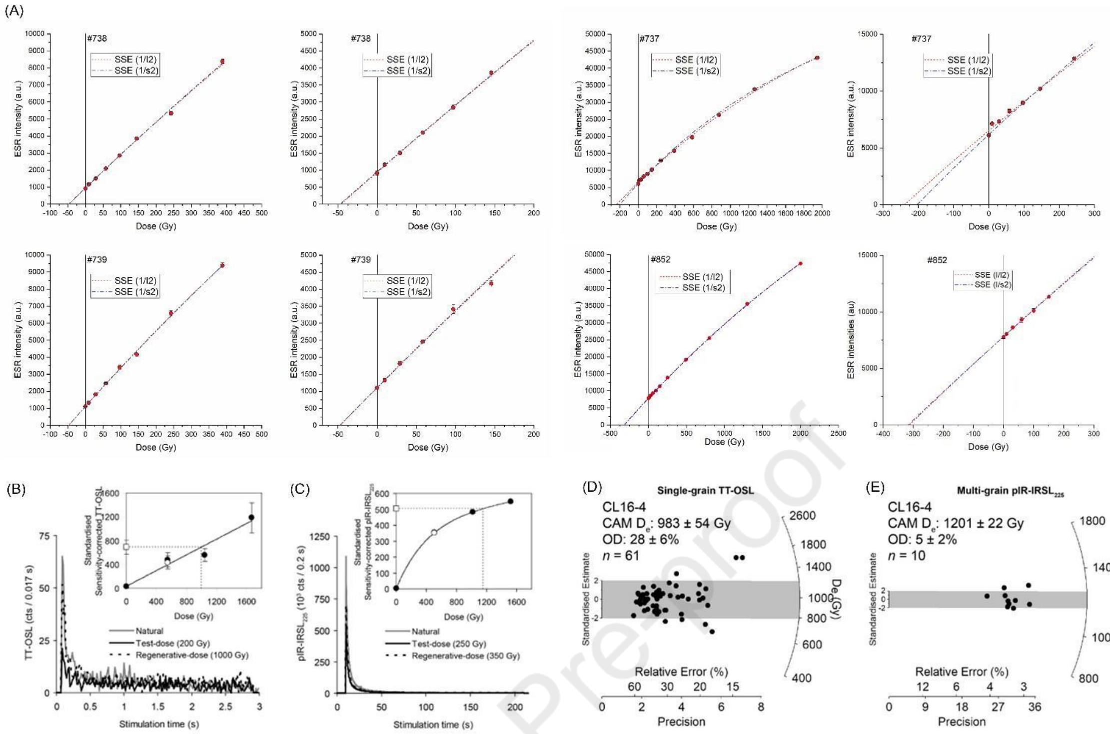
(A)
#738
#737
#739
#852
SSE (1/I2)
SSE (1/s2)
ESR intensity (a.u.)
Dose (Gy)
(B)
(C)
(D)
(E)
Single-grain TT-OSL
Multi-grain pIR-IRSL225
CL16-4
CAM De: 983 ± 54 Gy
OD: 28 ± 6%
n = 61
CAM De: 1201 ± 22 Gy
OD: 5 ± 2%
n = 10
Natural
Test-dose (200 Gy)
Regenerative-dose (1000 Gy)
Test-dose (250 Gy)
Regenerative-dose (350 Gy)
Stimulation time (s)
Standardised Estimate
Relative Error (%)
Precision
De (Gy)

Table 1

Sample	#738	#739	#737	#852
Site (Unit)	Galería Estatuas (LU4)	Galería Estatuas (LU4)	Cata Litario (LU5)	Cata Litario (LU5)
Species	*Equus sp.*	Cervidae	*Ursus deningeri*	*Ursus deningeri*
US-ESR[a] age (ka)	*	90 ± 9	217 ± 22	258 ± 21
CSUS-ESR[a] age (ka)	116 ± 12	92 ± 9	245 ± 31	273 ± 21
US-ESR[b] age (ka)	n.a	n.a	273 ± 28	280 ± 23
CSUS-ESR[b] age (ka)	n.a	n.a	**304 ± 33**	**287 ± 23**
US-ESR[c] age (ka)	**117 ± 13**[d] 118 ± 13[e]	**87 ± 9**[d]	**217 ± 21**[f] 227 ± 20[g]	**256 ± 24**[d]
AAR age (ka) (2 subsamples per tooth)	A: 175[†] B: 76[†]	A: 56[†] B: 67[†]	A: 364 B: 393	A: 125[†] B: 261
AAR mean age (ka)	n.a	n.a	378.3 ± 14.5	n.a

[a] Ages calculated with DATA program (Grün, 2009) considering post-Rn equilibrium in dental tissues. [b] Ages calculated with DATA program (Grün, 2009) considering post-Rn disequilibrium in dental tissues. [c] Ages calculated with USESR program (Shao et al., 2014) with post-Rn equilibrium. [d] Ages calculated with US models in all tissues (enamel and dentine and, if applies, cement) models. [e] Ages calculated with US (enamel)/US (dentine)/AU (cement) models. [f] Ages calculated with US (enamel) and AU (dentine) models. [g] Ages calculated with AU models in enamel and dentine. * = no finite US-ESR age can be obtained with DATA program (Grün, 2009). † = age not reliable (see text for explanations). n.a = not applicable. In bold, ages displayed on Fig. 2.

Table 2

		Single-grain TT-OSL [a]						Multi-grain pIR-IR$_{225}$ [e]					
Sample	Unit	Accepted/ measured grains	Grain size (μm)	OD (%) [b]	D_e (Gy) [c]	Total dose rate for Qz (Gy / ka)	Age (ka) [d]	Accepted/ measured aliquots	Grain size (μm)	OD (%) [b]	D_e (Gy) [c]	Total dose rate for K-feldspars (Gy / ka)	Age (ka) [d]
CL16-2	LU-4	32 / 2400	90-125	36 ± 8	912 ± 78	2.34 ± 0.15	389 ± 42	15 / 15	90-125	8 ± 2	1202 ± 29	2.80 ± 0.15	429 ± 27
CL16-1	LU-5	31 / 2200	90-125	20 ± 9	960 ± 69	2.44 ± 0.18	393 ± 41	10 / 10	90-125	6 ± 2	1202 ± 25	2.90 ± 0.18	414 ± 29
CL16-3	LU-5	26 / 3200	90-125	38 ± 8	943 ± 91	2.15 ± 0.14	439 ± 52	14 / 14	90-125	7 ± 2	1158 ± 24	2.61 ± 0.15	444 ± 28
CL16-4	LU-6	61 / 2500	63-90	28 ± 6	983 ± 52	2.68 ± 0.18	367 ± 32	10 / 10	63-90	5 ± 2	1201 ± 22	3.06 ± 0.18	393 ± 25

[a] TT-OSL measurements were made using the ‘pseudo’ single-grain approach (i.e., ~18 grains per hole; Arnold et al., 2012b).
[b] D_e values have been calculated using the central age model (CAM; Galbraith et al., 1999).
[c] Mean ± total uncertainty (68%a confidence interval), calculated as the quadratic sum of the random and systematic uncertainties. Total uncertainty includes a systematic component of ±2% associated with laboratory beta-source calibration.
[d] pIR-IRSL$_{225}$ measurements were made using ~160-grain aliquots.

Table 3

Sample (unit)	^{238}U (ppb)	^{232}Th (ppb)	^{230}Th / ^{232}Th (atomic x10^{-6})	$d^{234}U$* (measured)	^{230}Th / ^{238}U (activity)	^{230}Th Age (ka) (uncorr.)	^{230}Th Age (ka) (corr.)	$d^{234}U_{Initial}$** (corr.)	^{230}Th Age (ka)*** (corr.)
SCI18-A (LU2)	64.1 ± 0.1	7.5 ± 0.1	125 ± 3	45.6 ± 2.4	0.893 ± 0.004	203.3 ± 3.2	200.1 ± 3.8	80 ± 4	**200.1 ± 3.8**
SCI18-B (LU6)	402.6 ± 0.4	5.2 ± 0.1	1280 ± 26	49.5 ± 1.4	1.008 ± 0.002	318.4 ± 5.1	318.1 ± 5.1	122 ± 4	**318.0 ± 5.1**
SCI23-A (LU6)	336.9 ± 0.3	14.6 ± 0.3	379 ± 8	58.8 ± 1.2	0.998 ± 0.003	285.6 ± 4.5	284.5 ± 4.5	131 ± 3	**284.4 ± 4.5**
SCI23-B (LU5)	280.5 ± 0.6	23.2 ± 0.5	195 ± 4	28.6 ± 1.7	0.978 ± 0.004	312.2 ± 7.6	309.9 ± 7.6	69 ± 4	**309.9 ± 7.6**
SCI23-C1 (LU5)	286.2 ± 0.3	7.5 ± 0.1	652 ± 13	38.4 ± 0.3	1.035 ± 0.003	444.9 ± 18.8	444.2 ± 18.6	135 ± 8	**444.1 ± 18.6**
SCI23-C2 (LU5)	341.0 ± 0.4	7.7 ± 0.1	750 ± 15	34.2 ± 1.4	1.027 ± 0.002	433.7 ± 14.6	433.1 ± 14.6	116 ± 7	**433.1 ± 14.6**

U decay constants: $\lambda^{238} = 1.55125x10^{-10}$ (Jaffey et al., 1971) and $\lambda^{234} = 2.82206x10^{-6}$ (Cheng et al., 2013). Th decay constant: $\lambda^{230} = 9.1705x10^{-6}$ (Cheng et al., 2013).
*$\delta^{234}U = ([^{234}U/^{238}U]_{activity} - 1)x1000$. **$\delta^{234}U_{initial}$ was calculated based on ^{230}Th age (T), i.e., $\delta^{234}U_{initial} = \delta^{234}U_{measured}$ x $e^{\lambda 234xT}$.
Corrected ^{230}Th ages assume the initial $^{230}Th/^{232}Th$ atomic ratio of 4.4 ± 2.2 x10^{-6}. Those are the values for a material at secular equilibrium, with the bulk earth $^{232}Th/^{238}U$ value of 3.8 All errors are 2σ.

Declaration of interests

☒ The authors declare that they have no known competing financial interests or personal relationships that could have appeared to influence the work reported in this paper.

☐ The authors declare the following financial interests/personal relationships which may be considered as potential competing interests:

Virginia Martínez-Pillado
(corresponding author)
and co-authors